A New Class of Ultra-Low-Profile, Highly Flexible Antenna Arrays for the Fifth-Generation Millimeter-Wave Communication Band on Flexible Printed Circuit Board

Behzad Ashrafi Nia, Soheil Saadat, and Franco De Flaviis

Abstract – This article presents the design and experimental validation of two single-element flexible antennas, as well as the arrays operating near 28 GHz. The first design is a patch antenna with dual-polarized capability that is 202 μm thick. It is a capacitive coupled patch antenna with parasitic elements to improve scan range. This antenna covers 26.5 GHz to 28.3 GHz and has a 4.9 dBi peak gain with the measured cross polarization of more than 25 dB in the direction of the main beam. The second proposed antenna is a cavity slot antenna that is 202 μm thick. A measurement on the cavity slot antenna shows 1.55 GHz bandwidth between 27.6 GHz and 29.15 GHz and 4.6 dBi gain. The measured cross-polarization isolation at the broadside is around 35 dB. The two proposed antennas feature a low-profile, lightweight, and cost-efficient design, all of which are desirable characteristics for fifth-generation commercial applications.

1. Introduction

The fifth generation (5G) of mobile communication technology is considered a very attractive solution for exponentially expanding wireless data traffic in the future [1, 2] due to its ability to use significantly larger bandwidths at millimeter-wave frequencies. Moving to the millimeter-wave frequencies would bring new challenges partially related to the high frequency of operation and partially related to the design of small low-cost phased arrays to operate at those frequencies [3]. When operating at high frequencies, path loss could also become an issue. To overcome this obstacle, a small and flexible antenna array with high gain and the ability to generate dynamically directional beams is desirable. The ability of flex circuits to accommodate tightly bending radii and to eliminate the need for cables and connectors gives designers greater flexibility compared with traditional printed circuit board. It enables products and applications that would not otherwise be possible [4, 5]. Previous works demonstrates the use of a flexible antenna at low frequencies [6–9]. In this work, the potential of flexible substrates for high-frequency antennas for 5G applications is investigated. The second challenge in using a flexible material is associated with its thickness that normally provides very narrowband designs. Although some antenna concepts have been proposed for 5G wireless applications [10–13], to the best of the authors' knowledge, only a few antennas using a thin substrate with wideband and high gain, have been reported [14–16]. In this work, to address those two challenges, two types of compact and flexible antennas in single and linear array configurations operating at 28 GHz are presented.

Manuscript received 24 May 2022.

Behzad Ashrafi Nia and Franco De Flaviis are with the University of California, Henry Samueli School of Engineering, Irvine, California 92694, USA; e-mail: bashrafi@uci.edu, franco@uci.edu.

Soheil Saadat is with Multi-Fineline Electronix Inc., Irvine, California 92697, USA; e-mail: soheil2054@gmail.com.

2. Material Characterization and Accurate Electromagnetic Simulations for On-Wafer Measurement Setup

Although many substrates are treated as isotropic materials for design simplicity, in high-frequency applications they need to be more accurately characterized in case they exhibit some anisotropic properties [17–19]. This part of the article aims to accurately calculate the resonance frequency of the proposed antenna on the anisotropic flexible substrate. In this article, two thicknesses are investigated. The first one is 120 μm (quasi-Yagi–Uda antenna [20]), and the second one is 202 μm (cavity slot and patch antenna). The substrate used in this work is called Pyralux TA laminate, and based on the data sheet, the relative permittivity and loss tangent are 3.2 and 0.004 at 10 GHz, respectively.

To estimate the substrate effective dielectric constant, the resonance frequency of the quasi-Yagi–Uda antenna is recorded first. The real part of the dielectric material permittivity is extracted. To achieve this, the exact layout of two fabricated antennas is simulated by CST Studio Suite, version 2022, and S-parameter results are compared with measurement. The simulated and measured reflection coefficients (S_{11}) of the quasi-Yagi–Uda antenna are presented in Figure 2. After the analysis, a noticeable shift in the resonance frequency of the antenna is observed. This work allows variation in both ε_z (relative permittivity along the optical axis) and $\varepsilon_x = \varepsilon_y$ (relative permittivity along the two axes perpendicular to the optical axis) to investigate the substrate's anisotropy effects. After a few rounds of simulation, appropriate values for both ε_z and ε_x are extracted, and the S parameter is shown in Figure 2. The

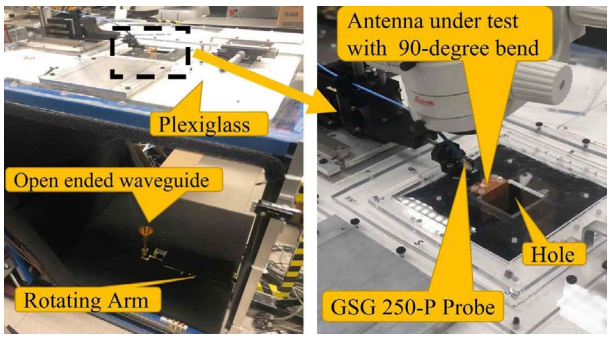

Figure 1. Far-field probe station setup.

effect of permittivity variation along the optical axis is more pronounced when the substrate is thinner. A similar approach is applied for the substrate with a thickness of 202 μm, and the best matched values are reported in Table 1.

Even though measurement and simulation matched very well by choosing the values in Table 1, there is still a shift in the value of S_{11} (Figure 2, simulation_method_1, red curve). The possible reason for the frequency shift can be the modeling of the ground–signal–ground (GSG) probe at millimeter-wave frequencies. An optimized version of the excitation setup, named *simulation_method_2*, is shown in Figure 3. Perfect electric conductor sheets are used to connect the lumped port to the ground planes. This simple setup can be used to replace the complex simulation model of the GSG probe with its cable. Method 2 results are perfectly matched with measurements (Figure 2, simulation method 2, green curve). The performance of the quasi-Yagi–Uda antenna is presented in our previous work [20].

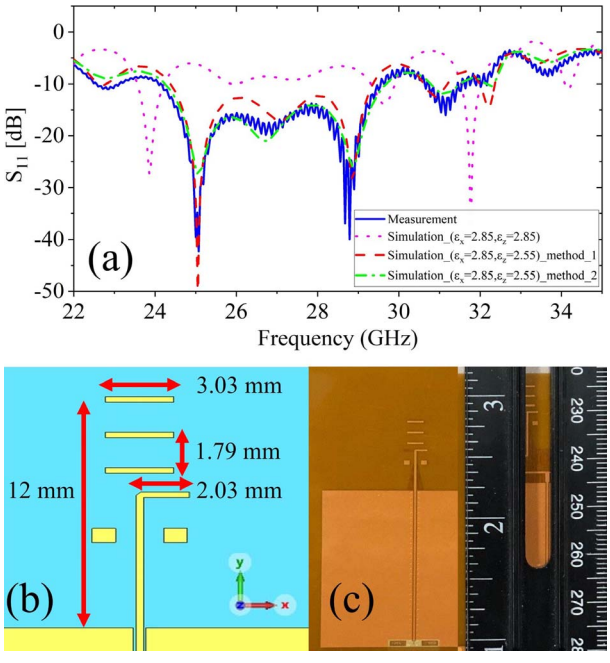

Figure 2. (a) The simulated S_{11} parameter of quasi-Yagi–Uda antenna for different scenarios. (b) Structure of the proposed antenna and (c) fabricated antenna in [20].

Table 1. Relative permittivity for different thicknesses

	Dielectric constant		
Thickness	ε_x	ε_y	ε_z
120 μm	3.2	3.2	2.55
202 μm	3.2	3.2	2.75

3. Proposed 5G Antennas and Results

The detailed design of each antenna is presented. These antennas are patch and cavity slot antennas. A picture of the measurement setup used to measure the radiation pattern is shown in Figure 1. More details of the measurement setup are discussed in [21].

3.1 Patch Antenna Design

The geometry for the patch antenna is introduced that is suitable for a thin substrate. The patch antenna is printed on a substrate that is 202 μm thick and is designed to resonate at 28 GHz. The geometry of the proposed antenna is depicted in Figure 4. To meet the requirement of the 5G millimeter-wave band and increase the bandwidth on such a thin substrate, a capacitive feeding method and parasitic rectangular elements around the main patch are implemented. The capacitive feeding method counteracts the inductance of the via that is connected to the embedded microstrip line under the main patch. To improve the bandwidth and gain of the antenna, four parasitic rectangular elements are added in the same layer [22, 23]. These parasitic elements can add a new resonance near the primary patch resonance and, as a result, increase the bandwidth. The overall size of the proposed patch antenna, including parasitic elements, is 6.3 mm × 6.3 mm. The optimized value of each parameter in Figure 4 is shown in Table 2.

A feed network comprised of microstrip lines and a T junction is used to integrate the patch in a 1 × 4 linear array. The size of the linear array is 6.3 mm × 27 mm, and element spacing is set to be 7 mm. The simulated and measured S parameter and gain results, as well as radiation pattern, are presented in Figures 5 and 6. The performance of both topologies is summarized in Table 4. The cross-polarization level is around 25 dB,

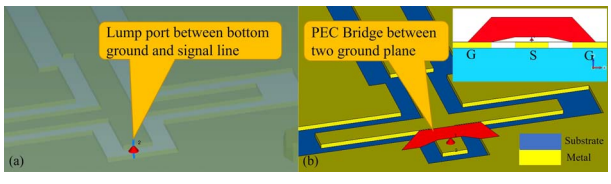

Figure 3. (a) Simulation setup for excitation of the Grounded Coplanar Waveguide (GCPW) line (method_1) and (b) simulation setup for excitation of the GCPW line (method_2).

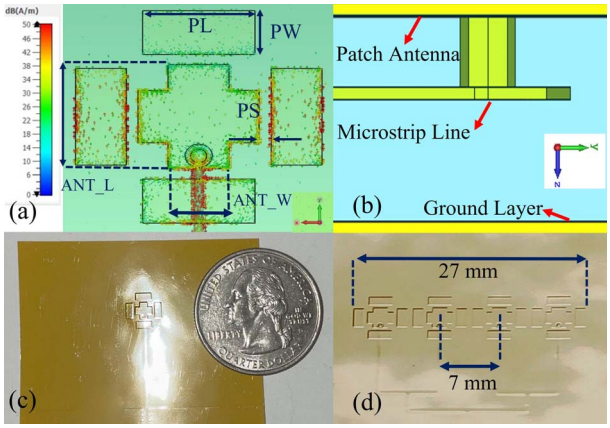

Figure 4. (a) The geometry and distribution of the current surface at the resonance frequency of the proposed antenna, (b) side view, and (c) and (d) fabricated single and array antennas.

and the maximum realized gain is 10.8 dBi for the array element.

3.2 Cavity Slot Antenna Design

An original millimeter-wave cavity slot antenna design is presented, as shown in Figure 7. The cavity slot antenna is also a good candidate for this frequency band due to its compact size, shielding, easy fabrication, and low profile. In addition, the cavity slot antenna is more compact and has better cross polarization compared with the proposed patch antenna. The cavity slot antenna is also etched on a substrate of 202 μm thickness. The circular ring slot is etched on the ground plane on the backside of the substrate. Ground vias are placed around the ring to connect the bottom ground layer to the top ground layer to create a cavity. The cavity is excited by a stripline feed. The feed line is extended and tapered beyond the slot to form a tuning stub. The initial design is a narrow gap ring slot that offers a high impedance and narrow bandwidth. However, because the substrate is very thin, it is very challenging to have a wideband antenna at this frequency. To overcome this issue, four stepped stub arms are etched with 90° separation to increase the bandwidth and create a symmetric structure to provide a big copolarization to cross-polarization ratio. These arms are shown in Figure 7a as ARC2 and ARC3.

A general expression for the resonance frequency of the stepped slot antenna can be given as

$$f = \frac{c}{4 \times L_A} \tag{1}$$

where c is the speed of the light and L_A is the active length of the slot. The first and second resonance of the

Table 2. Parameters of the patch antenna

ANT_L	ANT_W	Patch Length	Patch Width	Patch Space
3.25 mm	1.5 mm	3 mm	1.3 mm	0.45 mm

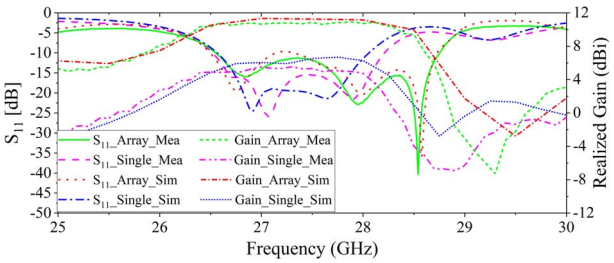

Figure 5. S parameter and realized gain of the proposed patch antenna versus frequency.

slot can be written as follows [24]:

$$L_{A1} = L_{S1} + 2 \times L_{S2} + 2 \times L_{S3} + 2 \times \frac{(W_{S2} - W_{S_1})}{2} + 2 \times \frac{(W_{S_3} - W_{S2})}{2} \tag{2}$$

$$L_{A2} = 2 \times \left(L_{S2} + L_{S3} + \frac{(W_{S2} - W_{S1})}{2} + \frac{(W_{S3} - W_{S2})}{2} \right) \tag{3}$$

where $L_{S1} = \frac{\mathrm{ANT}_D}{2} \times \mathrm{ARC1}$, $L_{S2} = \frac{\mathrm{ANT}_D}{2} \times \frac{\mathrm{ARC2-ARC3}}{2}$, and $L_{S3} = \frac{\mathrm{ANT}_D}{2} \times \frac{\mathrm{ARC3}}{2}$. The first and second resonance frequencies are set to be around 27 GHz and 28 GHz. By tuning the width and length (the portion is extended outward from the ring slot loop) of the stubs in the ring slot and stub of the feeding line, good impedance matching can be achieved by merging two resonance frequencies. This configuration gives a low level of cross polarization around 35 dB that is due to the symmetry of the electrical field across the aperture of radiation. The parameter values of the designed antenna are shown in Table 3. In addition, the cavity slot antenna is used in a four-element linear array. These antennas are spaced 6.5 mm from each other, and they

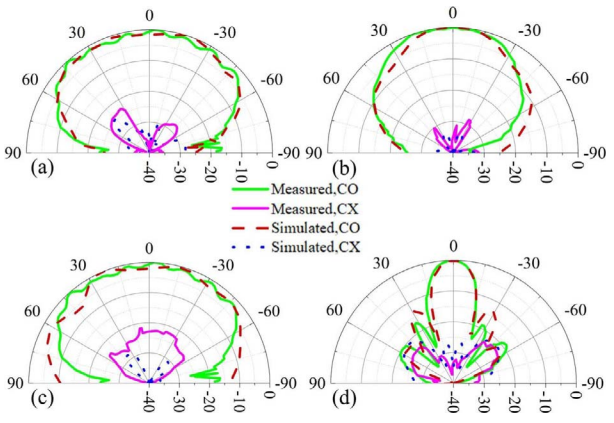

Figure 6. Simulated and measured radiation pattern of the proposed patch antenna at 28 GHz (a) E plane (single), (b) H plane (single), (c) E plane (array), and (d) H plane (array).

Table 3. Parameters of the cavity slot antenna

ANT_D	W_{S1}	W_{S2}	W_{S3}	ARC1	ARC2	ARC3
3.5 mm	0.09 mm	0.35 mm	0.508 mm	14°	76°	48°

Table 4. Specifications of the proposed antennas

Antenna	Type	Band Width (GHz)	Thickness (mm)	Maximum gain (dBi)	Efficiency (%)
Patch	Single	1.8	0.202	4.9	70
	Array	2.3	0.202	10.8	67
Cavity slot	Single	1.55	0.202	4.6	65
	Array	1.7	0.202	10.3	62

Table 5. Comparison proposed antennas with reported designs

Reference	Band Width (GHz)	Thickness (mm)	Gain (dBi)	Radiation pattern	Efficiency (%)
[10]	27.2–28.7	0.508	7.4	Boresight	N/A[a]
[11]	34–35.8	0.254	10–12	Boresight	60
[12]	20–36	0.6	10.24	Omnidirectional	67
[13]	21.7–33	0.2	9.7	Boresight	42

[a] Efficiency of the antenna is not reported in [10].

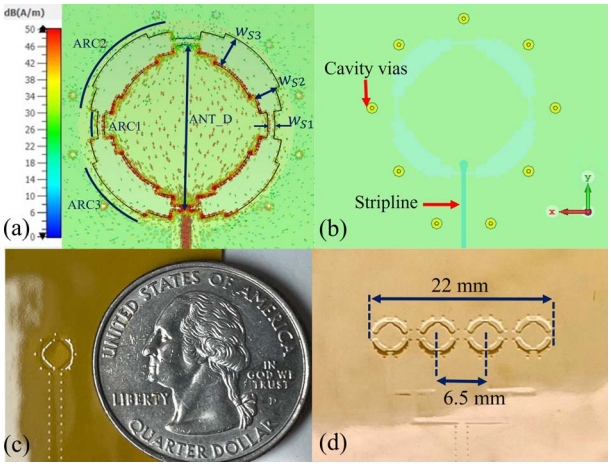

Figure 7. (a) The geometry and distribution of the current surface at the resonance frequency of the proposed antenna, (b) transparent top view, and (c) and (d) fabricated single and array antennas.

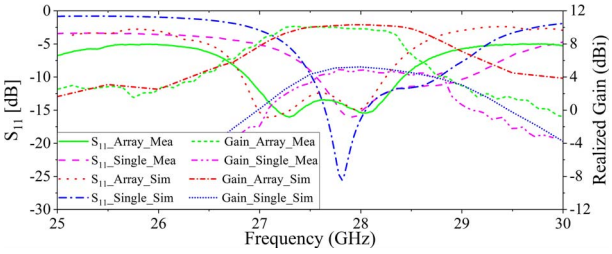

Figure 8. S parameter and realized gain of the proposed cavity slot antenna.

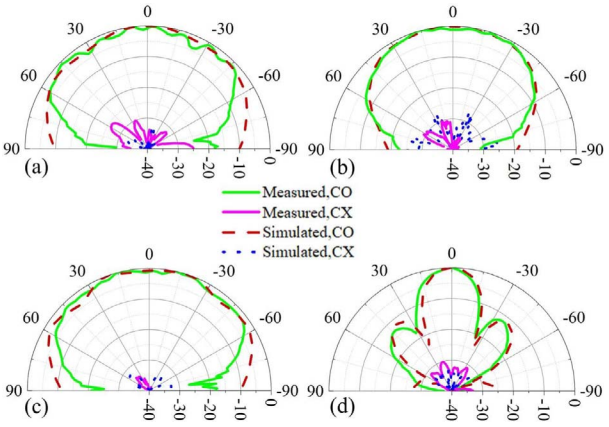

Figure 9. Simulated and measured radiation patterns of the proposed cavity slot antenna at 28 GHz (a) E plane (single), (b) H plane (single), (c) E plane (array), and (d) H plane (array).

are all simultaneously fed by on T-junction power divider.

The simulated and measured radiation pattern of the single and the array element are illustrated in Figure 9. According to the plots, the half-power beamwidth of a single element is 46° and 89° for the H plane and E plane, respectively, and 23° and 73° for the H plane and E plane, respectively, for the array element. Measured and simulated realized gain for the two types of antenna are plotted in Figure 8. The specifications of the performance of the antenna are presented in in Table 4.

4. Comparison and Conclusion

The main advantages of the proposed designs are 1) adequate bandwidth, 2) stable radiation patterns, 3) acceptable realized gain over the designated band, and 4) use of flexible material substrates. Therefore, valuable antenna designs are presented for the next generation of communications. A performance comparison of the proposed antennas with different recent published works for the frequencies of interest is shown in Table 5. The comparison proves that the proposed antennas excel in performance due to flexibility, bandwidth, a stable radiation pattern, and realized gain.

5. Acknowledgments

The authors acknowledge the support of Dassault Systèmes Simulia Corporation for providing the simulation software (CST Studio Suite). The authors are also thankful to Multi-Fineline Electronix Inc. for supporting this work and help in the fabrication of the antenna.

6. References

1. T. S. Rappaport, S. Sun, R. Mayzus, H. Zhao, Y. Azar, et al., "Millimeter Wave Mobile Communications for 5G Cellular: It Will Work!" *IEEE Access*, **1**, May 2013, pp. 335-349.
2. E. Hossain and M. Hasan, "5G Cellular: Key Enabling Technologies and Research Challenges," *IEEE Instru-*

mentation & Measurement Magazine, **18**, 3, June 2015, pp. 11-21.
3. T. S. Rappaport, R. W. Heath, Jr., R. C. Daniels, and J. N. Murdock, *Millimeter Wave Wireless Communications*, Upper Saddle River, NJ, Pearson Education, 2015.
4. G. Orecchini, M. M. Tentzeris, L. Yang, and L. Roselli, "'Smart Shoe'": An Autonomous Inkjet-Printed RFID System Scavenging Walking Energy," IEEE International Symposium on Antennas and Propagation (APSURSI), Spokane, WA, USA, July 3–8, 2011, pp. 1417-1420.
5. M. Ur-Rehman, N. A. Malik, X. Yang, Q. H. Abbasi, Z. Zhang, et al., "A Low Profile Antenna for Millimeter-Wave Body-Centric Applications," *IEEE Transactions on Antennas and Propagation*, **65**, 12, December 2017, pp. 6329-6337.
6. S. Das and D. Mitra, "A Compact Wideband Flexible Implantable Slot Antenna Design With Enhanced Gain," *IEEE Transactions on Antennas and Propagation*, **66**, 8, August 2018, pp. 4309-4314.
7. M. Tighezza, S. Rahim, and M. Islam, "Flexible Wideband Antenna for 5G Applications," *Microwave and Optical Technology Letters*, **60**, 1, January 2018, 2018, pp. 38-44.
8. S. Hong, S. H. Kang, Y. Kim, and C. W. Jung, "Transparent and Flexible Antenna for Wearable Glasses Applications," *IEEE Transactions on Antennas and Propagation*, **64**, 7, July 2016, pp. 2797-2804.
9. A. Dierck, H. Rogier, and F. Declercq, "A Wearable Active Antenna for Global Positioning System and Satellite Phone," *IEEE Transactions on Antennas and Propagation*, **61**, 2, February 2012, pp. 532-538.
10. J.-S. Park, J.-B. Ko, H.-K. Kwon, B.-S. Kang, B. Park, et al., "A Tilted Combined Beam Antenna for 5G Communications Using a 28-GHz Band," *IEEE Antennas and Wireless Propagation Letters*, **15**, January 2016, pp. 1685-1688.
11. Y. J. Cheng, H. Xu, D. Ma, J. Wu, L. Wang, et al., "Millimeter-Wave Shaped-Beam Substrate Integrated Conformal Array Antenna," *IEEE Transactions on Antennas and Propagation*, **61**, 9, September 2013, pp. 4558-4566.
12. Q. Jia, H. Xu, M. Xiong, B. Zhang, and J. Duan, "Omnidirectional Solid Angle Beam-Switching Flexible Array Antenna in Millimeter Wave for 5G Micro Base Station Applications," *IEEE Access*, **7**, October 2019, pp. 157027-157036.
13. H. Qiu, H. Liu, X. Jia, Z.-Y. Jiang, Y.-H. Liu, et al., "Compact, Flexible, and Transparent Antennas Based on Embedded Metallic Mesh for Wearable Devices in 5G Wireless Network," *IEEE Transactions on Antennas and Propagation*, **69**, 4, April 2021, pp. 1864–1873.
14. Y. J. Cheng, H. Xu, D. Ma, J. Wu, L. Wang, et al., "Millimeter-Wave Shaped-Beam Substrate Integrated Conformal Array Antenna," *IEEE Transactions on Antennas and Propagation*, **61**, 9, September 2013, pp. 4558-4566.
15. H.-L. Kao, C.-L. Cho, X. Y. Zhang, L.-C. Chang, B.-H. Wei, et al., "Bending Effect of an Inkjet-Printed Series-Fed Two-Dipole Antenna on a Liquid Crystal Polymer Substrate," *IEEE Antennas and Wireless Propagation Letters*, **13**, June 2014, pp. 1172-1175.
16. H.-L. Kao, C.-S. Yeh, X. Y. Zhang, C.-L. Cho, X. Dai et al., "Inkjet Printed Series-Fed Two-Dipole Antenna Comprising a Balun Filter on Liquid Crystal Polymer Substrate," *IEEE Transactions on Components, Packaging and Manufacturing Technology*, **4**, 7, July 2014, pp. 1228-1236.
17. N. G. Alexopoulos, "Integrated-Circuit Structures on Anisotropic Substrates," *IEEE Transactions on Microwave Theory and Techniques*, **33**, 10, October 1985, pp. 847–881.
18. N. G. Alexopoulos and C. M. Krowne, "Characteristics of Single and Coupled Microstrips on Anisotropic Substrates," *IEEE Transactions on Microwave Theory and Techniques*, **26**, 6, June 1978, pp. 387–393.
19. N. G. Alexopoulos and S. A. Maas, "Performance of Microstrip Couplers on an Anisotropic Substrate With an Isotropic Superstrata," *IEEE Transactions on Microwave Theory and Techniques*, **31**, 8, August 1983, pp. 671–674.
20. B. A. Nia, F. De Flaviis, and S. Saadat, "Flexible Quasi-Yagi-Uda Antenna for 5G Communication," 2021 IEEE International Symposium on Antennas and Propagation and USNC-URSI Radio Science Meeting (APS/URSI), Singapore, December 2021, pp. 115–116.
21. A. Hosseini, F. De Flaviis, and F. Capolino, "A 60 GHz Simple-to-Fabricate Single-Layer Planar Fabry–Pérot Cavity Antenna," *IET Microwave Antennas & Propagation*, **9**, 4, March 2015, pp. 313–318.
22. N. G. Alexopoulos and N. K. Uzunoglu, "A Simple Analysis of Thick Microstrip on Anisotropic Substrates (Technical Notes)," *IEEE Transactions on Microwave Theory and Techniques*, **26**, 6, June 1978, pp. 455–456.
23. S.-H. Wi, Y.-S. Lee, and J.-G. Yook, "Wideband Microstrip Patch Antenna WITH U-Shaped Parasitic Elements," *IEEE Transactions on Antennas and Propagation*, **55**, 4, April 2007, pp. 1196–1199.
24. R. Kumar, R. K. Khokle, and R. R. Krishna, "A Horizontally Polarized Rectangular Stepped Slot Antenna for Ultra Wide Bandwidth With Boresight Radiation Patterns," *IEEE Transactions on Antennas and Propagation*, **62**, 7, July 2014, pp. 3501-3510.